Unified approach to split absorbing boundary conditions for nonlinear Schrödinger equations

Jiwei Zhang,[1,*] Zhenli Xu,[2,†] and Xiaonan Wu[3,‡]
[1]*Department of Mathematics, Hong Kong Baptist University, Kowloon, Hong Kong, People's Republic of China*
[2]*Department of Mathematics and Statistics, University of North Carolina at Charlotte, Charlotte, North Carolina 28223, USA*
[3]*Department of Mathematics, Hong Kong Baptist University, Kowloon, Hong Kong, People's Republic of China*
(Received 14 May 2008; published 29 August 2008)

An efficient method is proposed for numerical solutions of nonlinear Schrödinger equations on an unbounded domain. Through approximating the kinetic energy term by a one-way equation and uniting it with the potential energy equation, absorbing boundary conditions are designed to truncate the unbounded domain, which are in nonlinear form and can perfectly absorb waves outgoing from the boundaries of the truncated computational domain. The stability of the induced initial boundary value problem defined on the computational domain is examined by a normal mode analysis. Numerical examples are given to illustrate the stable and tractable advantages of the method.

DOI: 10.1103/PhysRevE.78.026709 PACS number(s): 02.70.Bf, 03.75.Lm, 42.25.Gy

I. INTRODUCTION

In this paper, we consider the construction of absorbing boundary conditions (ABCs) for the nonlinear Schrödinger (NLS) equation,

$$i\hbar\frac{\partial\psi(x,t)}{\partial t}=\left[-\frac{\hbar^2}{2m}\frac{\partial^2}{\partial x^2}+V(x)+f(|\psi|^2)\right]\psi, \tag{1}$$

where m is the atomic mass, $\hbar$ represents the Planck constant, and $V(x)$ is the potential function. This equation appears in many fields of physical applications [1–3], such as the gravity waves on deep water in fluid dynamics, the pulse propagations in optics fibers, and the Bose-Einstein condensation (BEC). For the cubic nonlinearity $f(|\psi|^2)\psi=g|\psi|^2\psi$, Eq. (1) reduces to the well-known Gross-Pitaevskii equation, which has been studied by many different numerical methods, see [4–6] and references therein. Other nonlinearities such as the quintic nonlinearity [7] are also widely discussed.

A current challenge for numerical solutions of this kind of problem is due to the unboundedness of the physical domain. The common practice to overcome this difficulty is to limit the computational domain and solve a reduced problem. To make the truncated problems complete, boundary conditions should be added to the reduced problem. ABCs applied at prescribed artificial boundaries have been widely studied in recent decades [8–13] for various types of partial differential equations, see also the reviews [14–18]. The purpose of designing ABCs is to annihilate all the incident waves so that minor reflected waves may propagate back into the computational domain. ABCs can be distinguished into two categories: global ABCs and local ABCs. Global ABCs usually lead to the well-approximated and well-posed truncated problems, but the implementation cost is expensive. Fast evaluation methods [19,20] should be applied to treat global ABCs. On the other hand, local ABCs are computationally efficient, but accuracy and stability are the main concerns. There is another way to design ABCs based on the media of the material, called perfectly matched layer (PML) methods [21], which have been applied to many complicated wave propagation problems.

For nonlinear equations, however, it is difficult to find suitable artificial boundary conditions in general, except for some special cases such as the linearized problem [22], or the Burgers type questions [23–25] which can be connected with linear parabolic equations by the Cole-Hopf transformation. For the NLS equation on an unbounded domain, some approaches have been developed, mostly focusing on the cubic nonlinearity, for instance, Zheng [26] and Antonie *et al.* [27] derived its exact and approximate integrodifferential artificial boundary conditions, respectively. In [28,29], Szeftel developed the potential and the paralinear strategies for designing absorbing boundary conditions for one-dimensional nonlinear wave equations. Soffer and Stucchio [30] presented a phase space filter method to obtain ABCs. The PML [31,32] was also applied to handling the NLS equations. In recent papers [33,34], split local absorbing boundary (SLAB) conditions have been developed through a time-splitting procedure for one- and two-dimensional NLS equations. The local absorbing boundary conditions were imposed on the split linear subproblem and yielded a full scheme by coupling the discretizations for the interior equation and boundary subproblems. In addition, an adaptive method was developed to determine the parameter k_0 involved in the local boundary conditions. In this paper, we present an efficient implementation of the nonlinear absorbing boundary conditions for the NLS equation by making use of the splitting idea [33,34]. We distinguish incoming and outgoing waves along the boundaries for the linear kinetic subproblem, and then unite the potential energy subproblem to yield nonlinear boundary conditions which are of local form. We then examine that the coupling between the equation governing the wave in the computational domain and the boundary conditions on the artificial boundary is well posed. Furthermore, the obtained boundary conditions are "easy" to discretize and "cheap" to compute in terms of the computational cost. We will then perform numerical tests to illustrate the effectiveness and tractability of this approach.

*jwzhang@math.hkbu.edu.hk
†xuzl@ustc.edu
‡xwu@hkbu.edu.hk

II. NONLINEAR ABSORBING BOUNDARY CONDITIONS

A. Linear Schrödinger equation

Let us first consider the local ABCs of the linear Schrödinger equation,

$$i\hbar\frac{\partial\psi(x,t)}{\partial t}=-\frac{\hbar^2}{2m}\frac{\partial^2\psi}{\partial x^2}, \tag{2}$$

which will be the basis of constructing ABCs of nonlinear problems, because it is the kinetic part of the NLS equation (1). In the frequency domain of the Fourier transform, Eq. (2) can be written by

$$\frac{\hbar}{2m}\hat{\psi}_{xx}+\omega\hat{\psi}=0, \tag{3}$$

where the subscript represents the partial derivative, $\hat{\psi}(x,\omega)$ is the Fourier transform of $\psi(x,t)$ in time, and ω is the frequency. Equation (3) is homogeneous and has two linearly independent eigensolutions: $\hat{\psi}^{(1)}=e^{-i\sqrt{2m\omega/\hbar}x}$ for the left-going waves and $\hat{\psi}^{(2)}=e^{i\sqrt{2m\omega/\hbar}x}$ for the right-going waves. Because initially we truncate the domain such that the wave function $\psi(x,0)=0$ outside the computational domain, there is no incoming waves on the boundaries. The one way equations at the two boundaries, which can annihilate all the outgoing waves, are described by

$$i\sqrt{\frac{\hbar}{2m}}\hat{\psi}_x\pm\sqrt{\omega}\hat{\psi}=0, \tag{4}$$

where the plus sign in "±" corresponds to the right boundary condition, and the minus sign corresponds to the left. The transparent boundary conditions in the exact manner of the problem is then derived by an inverse Fourier transform:

$$i\sqrt{\frac{\hbar}{2m}}\psi_x\pm\frac{e^{-(\pi/4)i}}{\sqrt{\pi}}\frac{d}{dt}\int_0^t\psi(x,\tau)\frac{d\tau}{\sqrt{t-\tau}}=0, \tag{5}$$

which is a nonlocal boundary condition. In order to get local boundary conditions, a usual way is to approximate the square root $\sqrt{\omega}$ by using polynomials or rational polynomials. For instance, applying the approximations

$$\sqrt{\omega}=\sqrt{\omega_0}+O(\omega-\omega_0), \tag{6}$$

$$\sqrt{\omega}=\frac{\sqrt{\omega_0}}{2}+\frac{\omega}{2\sqrt{w_0}}+O(\omega-\omega_0)^2, \tag{7}$$

$$\sqrt{\omega}=\frac{\sqrt{\omega_0}(3\omega+\omega_0)}{\omega+3\omega_0}+O(\omega-\omega_0)^3, \tag{8}$$

we obtain the first three absorbing boundary conditions in the physical domain:

$$\text{1st order:}\quad i\sqrt{\frac{\hbar}{2m}}\frac{\partial\psi}{\partial x}\pm k_0\psi=0,$$

$$\text{2nd order:}\quad i\psi_t\pm i\sqrt{\frac{2\hbar}{m}}k_0\frac{\partial\psi}{\partial x}+k_0^2\psi=0,$$

$$\text{3rd order:}\quad \frac{3i\hbar k_0^2}{m}\frac{\partial\psi}{\partial x}-2\frac{\partial^2\psi}{\partial x\partial t}\pm\left(\frac{\hbar k_0^3}{m}\psi+6ik_0\frac{\partial\psi}{\partial t}\right)=0. \tag{9}$$

Here, ω_0 is a positive constant, and $k_0=\sqrt{\omega_0}$ which is called the wave-number parameter.

B. Nonlinear absorbing boundary conditions

In this section, we derive the absorbing boundary conditions for the one-dimensional NLS equation (1) on the region $\Omega=[x_l,x_r]$ by assuming that there do not exist incoming waves at the two ends x_l and x_r. We remark that this assumption is not correct for a general wave due to the nonlinear or space-dependent potential [35], but it is reasonable for many situations of physical applications; in fact, this is a fundamental assumption so that we can design absorbing boundary conditions.

To understand the philosophy of obtaining nonlinear absorbing boundary conditions, let us rewrite Eq. (1) into the following operator form:

$$i\hbar\frac{\partial\psi(x,t)}{\partial t}=[\hat{T}+\hat{V}]\psi(x,t), \tag{10}$$

where $\hat{T}$ represents the linear differential operator which accounts for the kinetic energy part, and $\hat{V}$ is the nonlinear operator that governs the effects of the potential energy and nonlinearity. These are given by

$$\hat{T}=-\frac{\hbar^2}{2m}\frac{\partial^2}{\partial x^2}\quad\text{and}\quad\hat{V}=V(x)+f(|\psi|^2). \tag{11}$$

In a time interval from t to $t+\tau$ for small τ, the solution of Eq. (10) can be approximated by

$$\psi(x,t+\tau)\approx e^{-i[\hat{T}+\hat{V}]\tau/\hbar}\psi(x,t)\approx e^{-i\hat{T}\tau/\hbar}e^{-i\hat{V}\tau/\hbar}\psi(x,t). \tag{12}$$

This means in a small time step τ that the approximation carries out the wave propagation in a kinetic energy step and a potential energy step separately. This is the basic idea of the well-known time-splitting method (or the split-step method) which is effective to numerically solve the nonlinear Schrödinger-type equations.

Since we have assumed that there are no incoming waves on the artificial boundaries x_l and x_r, noticing formulas (9), the kinetic operator $\hat{T}$ can be approached by one-way operators

$$\hat{T}\approx\hat{T}^{(2)}=-\hbar\left(\pm i\sqrt{\frac{2\hbar}{m}}k_0\frac{\partial}{\partial x}+k_0^2\right), \tag{13}$$

$$\hat{T}\approx\hat{T}^{(3)}=-\hbar^2\left(2i\frac{\partial}{\partial x}\pm 6k_0\right)^{-1}\left(\frac{3ik_0^2}{m}\frac{\partial}{\partial x}\pm\frac{k_0^3}{m}\right), \tag{14}$$

which correspond to the second- and third-order local boundary conditions in Eq. (9), respectively. Here, we also take the positive sign in "±" at $x=x_r$ and take the negative sign at x_l.

Substituting $\hat{T}^{(n)}$ for $\hat{T}$ in Eq. (12) yields approximating operators to the solution operator as follows:

$$e^{-i[\hat{T}+\hat{V}]\tau/\hbar} \approx e^{-i[\hat{T}^{(n)}+\hat{V}]\tau/\hbar}, \tag{15}$$

which imply the one-way equations,

$$i\hbar\frac{\partial\psi(x,t)}{\partial t} = [\hat{T}^{(n)} + \hat{V}]\psi(x,t). \tag{16}$$

They approximate Eq. (10) at two boundaries and can act as absorbing boundary conditions we need. Concretely, we obtain nonlinear absorbing boundary conditions:

$$n=2: \quad i\hbar\frac{\partial\psi}{\partial t} = \left[-\hbar\left(\pm i\sqrt{\frac{2\hbar}{m}}k_0\frac{\partial}{\partial x} + k_0^2\right) + V(x) + f(|\psi|^2)\right]\psi, \tag{17}$$

$$n=3: \quad i\hbar\left(2i\frac{\partial}{\partial x} \pm 6k_0\right)\frac{\partial\psi}{\partial t} = \left[-\frac{\hbar^2}{m}\left(3ik_0^2\frac{\partial}{\partial x} \pm k_0^3\right) + \{V(x) + f(|\psi|^2)\}\left(2i\frac{\partial}{\partial x} \pm 6k_0\right)\right]\psi. \tag{18}$$

Here, in order to increase the accuracy of the boundary conditions, the wave-number parameter k_0 is a function of time t, which will be determined by a windowed Fourier transform method [34] based on the frequency property of the wave function near the artificial boundaries. We express the boundary conditions (17) and (18) in the operator forms:

$$\mathbb{B}_-^{(n)}(x,t)\psi(x,t) = 0, \tag{19}$$

$$\mathbb{B}_+^{(n)}(x,t)\psi(x,t) = 0, \tag{20}$$

where $\mathbb{B}_-$ and $\mathbb{B}_+$, respectively, represent the left and right boundary conditions; that is, the minus sign in "$\pm$" is taken for $\mathbb{B}_-$, and the plus sign for $\mathbb{B}_+$. The initial value problem on the open domain of Eq. (1) restricted to the truncated interval $[x_l,x_r]$ is then approximated by an initial boundary value problem with local absorbing boundary conditions:

$$i\hbar\frac{\partial\psi(x,t)}{\partial t} = \left[-\frac{\hbar^2}{2m}\frac{\partial^2}{\partial x^2} + V(x) + f(|\psi|^2)\right]\psi, \quad \text{for } x \in [x_l,x_r], \tag{21}$$

$$\psi(x,0) = \psi_0(x), \quad \text{for } x \in [x_l,x_r], \tag{22}$$

$$\mathbb{B}_-^{(n)}(x_l,t)\psi(x_l,t) = 0, \quad \text{for } n=2 \text{ or } 3, \tag{23}$$

$$\mathbb{B}_+^{(n)}(x_r,t)\psi(x_r,t) = 0, \quad \text{for } n=2 \text{ or } 3. \tag{24}$$

C. Well-posedness of the induced initial boundary value problem

It is natural to examine the well-posedness that we concern most of the induced initial boundary value problem confined in the finite computational interval for the nonlinear Schrödiger equation by using the nonlocal absorbing boundary condition. The classical energy method seems to be difficult to obtain the stability result of the problem under consideration here. In this section, we will investigate the stability based on Kreiss's normal mode analysis method [36,37], which was also used for the wave equations and the linear Schrödinger equation.

The idea of the general algebraic normal mode analysis is based on the fact that the well-posed problem does not admit any complex eigenvalues with positive real parts $\mathrm{Re}(s)>0$, or generalized eigenvalues with $\mathrm{Re}(s)=0$ and the negative (positive) group velocity of the normal mode on the right-hand (left-hand) boundary. The eigenvalues and generalized eigenvalues satisfy the dispersion relations of both the interior equation and the equation on the boundaries. If there exist such eigenvalues, the problem will admit an unboundedly grown normal mode e^{st} and is hence unstable. If there exist such generalized eigenvalues, the boundary conditions will admit an incoming wave which will propagate energy into the interior domain to disrupt the solution in the computational interval and generate a spurious wave solution.

We need to check if there exist eigenvalues and generalized eigenvalues by replacing the solution of the plane wave form $\psi(x,t)=e^{st+kx}$ into Eq. (21) and boundary conditions (23) and (24). There are left-hand and right-hand boundaries; they can be considered by the same argument. Here we only consider the well-posedness with the right-hand boundary conditions. For $n=2$, substituting the plane wave into the equation and the boundary condition yields

$$i\hbar s = -\frac{\hbar^2}{2m}k^2 + [V(x) + f(|\psi|^2)], \tag{25}$$

$$i\hbar s = -i\hbar\sqrt{\frac{2\hbar}{m}}k_0 k - \hbar k_0^2 + [V(x) + f(|\psi|^2)]. \tag{26}$$

In very small time step τ the basic idea of the well-known time-splitting method is to carry out the wave propagation in a kinetic energy step and a potential energy step separately. When the time step tends to zero, we can write the nonlinear Schrödinger equation in the above forms; the nonlinear term is considered as a potential function. Hence let Eq. (25) minus Eq. (26) and substitute the result into Eq. (25) to arrive at

$$k = i\sqrt{\frac{2m}{\hbar}}k_0 \quad \text{and} \quad s = -ik_0^2 - i\frac{v_1+f_1}{\hbar} + \frac{v_2+f_2}{\hbar}, \tag{27}$$

where $V+f=v_1+f_1+i(v_2+f_2)$. For the third-order approximation on the right boundary, by the same argument, we have

$$i\hbar s = -\frac{\hbar^2}{2m}k^2 + [V(x) + f(|\psi|^2)], \tag{28}$$

$$i\hbar s = -\frac{\hbar^2 k_0^2}{2m}\frac{3ik+k_0}{ik+3k_0} + [V(x) + f(|\psi|^2)]. \tag{29}$$

Combining Eqs. (28) and (29), we have

$$\frac{\hbar^2}{2m}k^2 - \frac{\hbar^2 k_0^2}{2m}\frac{3ik + k_0}{ik + 3k_0} = 0. \tag{30}$$

Solving Eq. (30) and substituting the results $k=ik_0$ into Eq. (28), we obtain

$$s = -i\frac{\hbar}{2m}k_0^2 - \frac{i[V(x) + f(|\psi|^2)]}{\hbar}, \tag{31}$$

$$s = -i\frac{\hbar}{2m}k_0^2 - i\frac{v_1 + f_1}{\hbar} + \frac{v_2 + f_2}{\hbar}. \tag{32}$$

It is easy to see that $\mathrm{Re}(s) \leqslant 0$ for $v_2+f_2 \leqslant 0$ from Eqs. (27) and (32), which correspond to the second- and third-order ABCs, respectively.

In particular, when V and f are both real functions, i.e., $v_2+f_2=0$, we thus have $\mathrm{Re}(s)=0$, hence s is wholly imaginary. Since the boundary condition is designed to annihilate all the outgoing wave, this implies that the group velocity is positive on the right-hand boundary. Hence there is no generalized eigenvalue which will propagate energy into the interior interval to influence the true wave solution. If any instabilities which might be admitted by the generalized eigenvalues of the ABCs exist, they would not propagate the wave to affect the interior solution. Keeping this concept in mind, by linearizing the nonlinear terms in a sufficiently small time step, we can say that the boundary conditions of the problem (21)–(24) are well posed if functions $V(\cdot)$ and $f(\cdot)$ satisfy $v_2+f_2 \leqslant 0$. Hence the boundary condition for $n=2$ or 3 is well posed and numerical tests below show that the boundary condition is stable.

III. NUMERICAL EXAMPLES

In this section we will test the effectiveness of the nonlinear absorbing boundary conditions by using the finite-difference scheme to the induced initial boundary value problem (21)–(24). In the computational interval $[x_l, x_r]$, let J be a positive integer, and denote $\Delta x=(x_r-x_l)/J$ and Δt by grid sizes in space and time, respectively. We use the following Crank-Nicolson-type difference scheme [38–40]:

$$i\hbar\frac{\psi_j^{n+1} - \psi_j^n}{\Delta t} = -\frac{\hbar^2}{2m}\frac{\psi_{j+1}^{n+1/2} - 2\psi_j^{n+1/2} + \psi_{j-1}^{n+1/2}}{\Delta x^2} + \left[V_j + f\left(|\psi^{n+1/2}|^2\right)\right]\psi_j^{n+1/2}, \tag{33}$$

to discretize the NLS equation inside the computational domain, which is unconditionally stable and of second order of accuracy in both space and time. Here $\psi_j^{n+1/2}=\frac{\psi_j^{n+1}+\psi_j^n}{2}$, and ψ_j^n represents the approximation of wave function ψ at the grid point (x_j, t^n) with $j=0,1,\ldots,J$, $x_0=x_l$, $x_j=x_l+j\Delta x$, $x_J=x_r$, and $t^n=n\Delta t$. Obviously, the above systems of equations cannot be solved uniquely since the number of equations are less than that of unknowns. At the two unknown ghost points x_{-1} and x_{J+1} no equation can be defined from Eq. (33). Thus the absorbing boundary conditions are required to provide two extra equations on the grid points x_s for $s \in S = \{-1,0,1\} \cup \{J-1, J, J+1\}$ in the vicinity of the boundary. The third-order ABCs are discretized as follows:

$$\left[\frac{3\hbar^2 k_0^2 i}{m} - 2i(V_s + f(|\psi_s^{n+1/2}|^2)\right]\frac{\psi_{s+1}^{n+1/2} - \psi_{s-1}^{n+1/2}}{2\Delta x} - \hbar\frac{\psi_{s+1}^{n+1} - \psi_{s-1}^{n+1}}{\Delta x \Delta t} + \hbar\frac{\psi_{s+1}^{n} - \psi_{s-1}^{n}}{\Delta x \Delta t} \pm 6k_0 i\frac{\psi_s^{n+1} - \psi_s^n}{\Delta t} \pm \left(\frac{\hbar^2 k_0^3}{m} - 6k_0 V_s - 6k_0 f(|\psi_s^{n+1/2}|^2)\right)\psi_s^{n+1/2} = 0, \tag{34}$$

where the positive sign in "±" corresponds to the right boundary $s=J$ and the negative one corresponds to the left boundary $s=0$. The above scheme is implicit, and we need to use an iterative strategy to solve the nonlinear equations (33) and (34) by replacing $f(|\psi_j^{n+1/2}|^2)$ with $f(|\frac{(\psi_j^{n+1})^k+\psi_j^n}{2}|^2)$, where the superscript k denotes the kth iteration at each time step and the initial iteration is given by $(\psi_j^{n+1})^0=\psi_j^n$.

Without loss of generality, we rewrite the original NLS equation (1) as

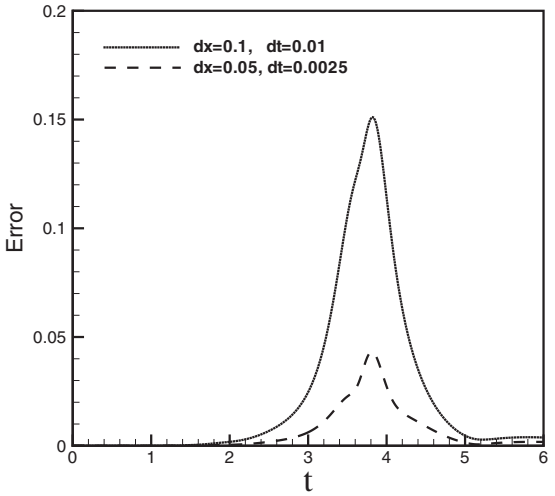

FIG. 1. Evolution of the error $|\psi_{exa}-\psi_h|$ on the artificial boundary point.

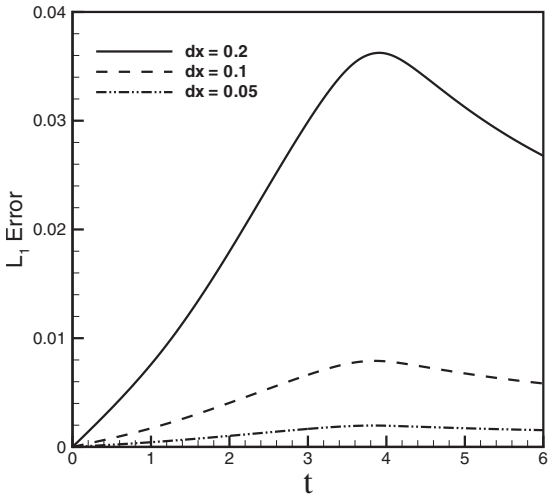

FIG. 2. L_1 errors vs time t with refinement meshes.

TABLE I. The L_1 errors and orders for different times and mesh sizes.

	$\Delta x=0.2$	Order	$\Delta x=0.1$	Order	$\Delta x=0.05$	Order
$t=2$	1.570×10^{-2}		4.149×10^{-3}	2.076	1.017×10^{-3}	2.029
$t=3$	2.946×10^{-2}		6.797×10^{-3}	2.116	1.656×10^{-3}	2.037
$t=4$	3.622×10^{-2}		8.091×10^{-3}	2.162	1.955×10^{-3}	2.049
$t=5$	3.145×10^{-2}		6.948×10^{-3}	2.178	1.724×10^{-3}	2.011
$t=6$	2.691×10^{-2}		6.010×10^{-3}	2.163	1.581×10^{-3}	1.926

$$i\psi_t = -\psi_{xx} + gf(|\psi|^2)\psi + V\psi, \tag{35}$$

where $gf(|\psi|^2)\psi$ represents different physical significance when different nonlinear forms are chosen. In example 1, we take $f(|\psi|^2)=|\psi|^2$, $V=0$, and $g=-2$, which corresponds to a focusing ($g<0$) effect of the cubic nonlinearity. Many applications in science and technology have connections with this kind of NLS equation [1–3]. Furthermore, in this case Eq. (35) can be solved analytically by the inverse scattering theory; its one soliton solution has the following form:

$$\psi(x,t) = A\sqrt{\frac{-2}{g}}\,\mathrm{sech}(Ax - 2ABt)e^{iBx+i(A^2-B^2)t}, \tag{36}$$

where A and B are real parameters: A determines the amplitude of the wave field, and B is related to velocity of the soliton. In example 2, we take $f(|\psi|^2)=|\psi|^4$, $V=0$, and $g=-2$; the NLS equation becomes a quintic nonlinearity. The computational interval is set to be $[x_l,x_r]=[-5,5]$. For this kind of NLS equation with powerlike nonlinearity, if the initial energy satisfies

$$E(\psi_0) := \|\nabla\psi_0\|_{L^2}^2 - \frac{2}{3}\|\psi_0\|_{L^6}^6 < 0, \tag{37}$$

the solution ψ will blow up in finite time ([41] and references therein), i.e., there exists $T>0$ such that

$$\lim_{t\to T}\|\nabla_x\psi\|_{L^2} \to +\infty.$$

In example 3, we take $f(|\psi|^2)=|\psi|^2$, $V\neq0$, and $g=2$. In this setting, the NLS equation represents a nonlinear wave with repulsive interaction.

Example 1. We first consider the case of $g=-2$ and the temporal evolution of an initial bright soliton,

$$\psi(x,0) = \mathrm{sech}(x-x_0)e^{2i(x-x_0)}, \tag{38}$$

with $x_0=15$. The exact solution is the form of Eq. (36) with $A=1$ and $B=2$. This case is used to test the performance of the nonlinear ABCs when the wave impinges on the right boundary of the computational interval [0,30]. Figure 1 shows the evolution of absolute error $|\psi_{exa}-\psi_h|$ on the artificial boundary point by picking wave number $k_0=2$, spatial size $\Delta x=0.1$, and time size $\Delta t=0.01$, and their refined sizes. When refining the mesh, one can see that the error converges quickly. In order to explore the convergence rates in space and time, we take the time size as $\Delta t=\Delta x^2$. Denote the L_1 error by

$$E_1(\Delta x) = \frac{1}{(J+1)(N+1)}\sum_{j=0}^{J}\sum_{n=0}^{N}|\psi_j^n - \psi_{exa}(x_j,t^n)|. \tag{39}$$

Figure 2 shows the evolution of the L_1 error with different mesh sizes. From this figure, we observe a second-order accuracy of the errors. To characterize convergence rates exactly, we take the different values of the L_1 norm at different times and mesh sizes. To compute the convergence rate, we use the formula

$$\text{rate} = \log_2\left(\frac{E_1(\Delta x)}{E_1(\Delta x/2)}\right).$$

Table I shows the second-order convergence rate.

TABLE II. The reflection ratios for $\Delta x=2\Delta t=0.1$, $g=-2$ or -10 and different parameter k_0.

$g\backslash k_0$	0.5	0.75	1.0	1.25	1.5	1.75	2.0	2.125	2.25
−2	6.07×10^{-2}	1.601×10^{-2}	4.70×10^{-3}	1.52×10^{-3}	5.17×10^{-4}	1.81×10^{-4}	7.30×10^{-5}	6.13×10^{-5}	7.06×10^{-5}
−10	6.07×10^{-2}	1.60×10^{-2}	4.70×10^{-3}	1.52×10^{-3}	5.17×10^{-4}	1.81×10^{-4}	7.30×10^{-5}	6.13×10^{-5}	7.05×10^{-5}
$g\backslash k_0$	2.5	2.75	3.0	3.25	3.5	3.75	4.0	4.25	4.5
−2	1.51×10^{-4}	3.23×10^{-4}	6.10×10^{-4}	1.04×10^{-3}	1.62×10^{-3}	2.40×10^{-3}	3.39×10^{-3}	4.60×10^{-3}	6.06×10^{-3}
−10	1.51×10^{-4}	3.23×10^{-4}	6.10×10^{-4}	1.03×10^{-3}	1.62×10^{-3}	2.40×10^{-3}	3.39×10^{-3}	4.60×10^{-3}	6.06×10^{-3}
$g\backslash k_0$	4.75	5.0	5.25	5.5	5.75	6.0	6.25	6.5	6.75
−2	7.77×10^{-3}	9.73×10^{-3}	1.20×10^{-2}	1.44×10^{-2}	1.72×10^{-2}	2.02×10^{-2}	2.34×10^{-2}	2.69×10^{-2}	3.05×10^{-2}
−10	7.77×10^{-3}	9.73×10^{-3}	1.20×10^{-2}	1.44×10^{-2}	1.72×10^{-2}	2.02×10^{-2}	2.34×10^{-2}	2.69×10^{-2}	3.05×10^{-2}

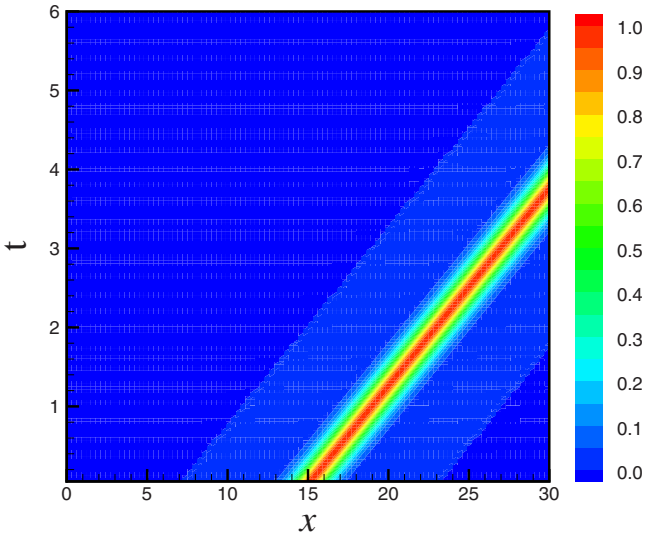

FIG. 3. (Color online) Evolution of the amplitude of the bright soliton with $k_0=2.0$.

Another important method to see the influence of k_0 on the boundary conditions is to show the reflection ratios [36,42] defined by

$$r = \sum_{j=0}^{J} |\psi_j^n| \Big/ \sum_{j=0}^{J} |\psi_j^0|, \tag{40}$$

which is efficient to measure the performance of the nonlinear ABCs. $r=0$ implies that the soliton passes through the boundary completely, and $r=1$ indicates that the wave is completely reflected back into the computational domain. In the experiments of Bose-Einstein condensations (BECs), g often takes a large value so that the nonlinear effect will become very strong. Table II presents the reflection ratios with parameter g being chosen as -2 and -10, respectively. We observe the influence of the wave numbers k_0 on the reflection ratios for spatial size $\Delta x=0.1$ and time size $\Delta t=0.05$. The reflection ratio r is insensitive to k_0, which can be taken in a large interval $[1.0, 5.0]$ such that the reflection ratios is less than 1%. Out of the interval, however, r will increase rapidly. Furthermore, whether the parameter g is given large or small, i.e., whether the nonlinear effect is strong or not, the reflection ratios is also insensitive. The ABCs can work well even when parameter g is chosen to be a large number. Figure 3 plots the amplitude of the soliton under $k_0=2.0$ and spatial size $\Delta x=0.1$, respectively. No observable reflections can be detected at all.

Example 2. We consider the quintic NLS equation with the initial value

$$\psi_0 = e^{-x^2+ik_0x},$$

where the wave number $k_0=8$. A direct calculation obtains the initial energy $E(\psi_0)\approx 80.5478>0$, which implies that the numerical experiment will not blow up. By using the Crank-Nicolson scheme proposed by Durán *et al.* [40], Fig. 4 shows the reflection ratios for different wave numbers under spatial size $\Delta x=0.1$ and its refinement $\Delta x=0.05$, respectively. Comparing the two curves, we can see that the reflection ratios decrease fast when the wave number is taken in the vicinity of the initial wave number $k_0=8$. And the reflection ratios in the coarse mesh is larger than those in the finer mesh when $k_0<4$. This indicates that the parameter k_0 in the nonlinear ABCs should be given in a suitable way. We can also see that if k_0 is equal to half of the group velocity of the wave impinged on the boundary point for the third-order case, the nonlinear ABCs will not disrupt the interior solution when the mesh is fine. Figure 5 shows the wave amplitude of utilizing the Crank-Nicolson method proposed by Durán under mesh size $\Delta x=0.01$, $\Delta t=0.001$, and $k_0=8.0$. The reflecting wave cannot be observed and the reflection ratio is 7.637×10^{-5}.

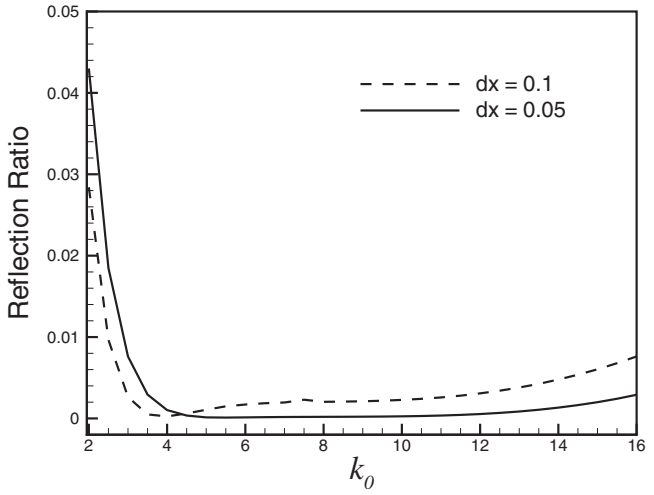

FIG. 4. The reflection ratios when different wave numbers k_0 are chosen under mesh $\Delta x=0.1$, 0.2.

Example 3. We consider a nonlinear wave for repulsive interaction with $g=2$ in Eq. (35). The initial data and potential function are taken to be Gaussian pulses,

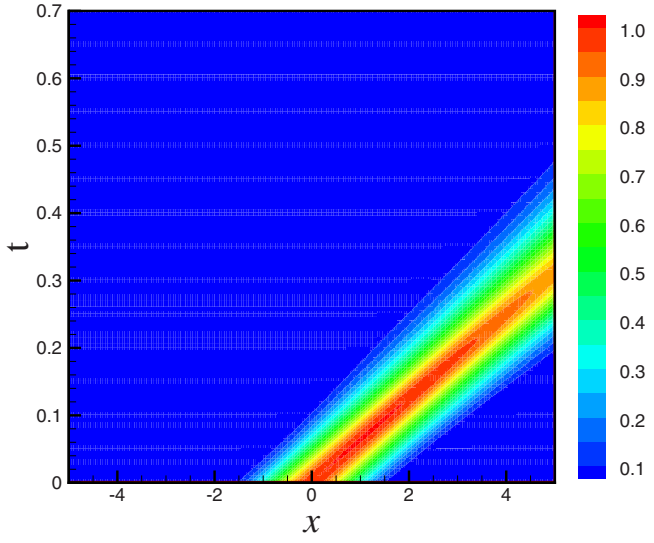

FIG. 5. (Color online) Evolution of the amplitude of the wave for the quintic NLS equation.

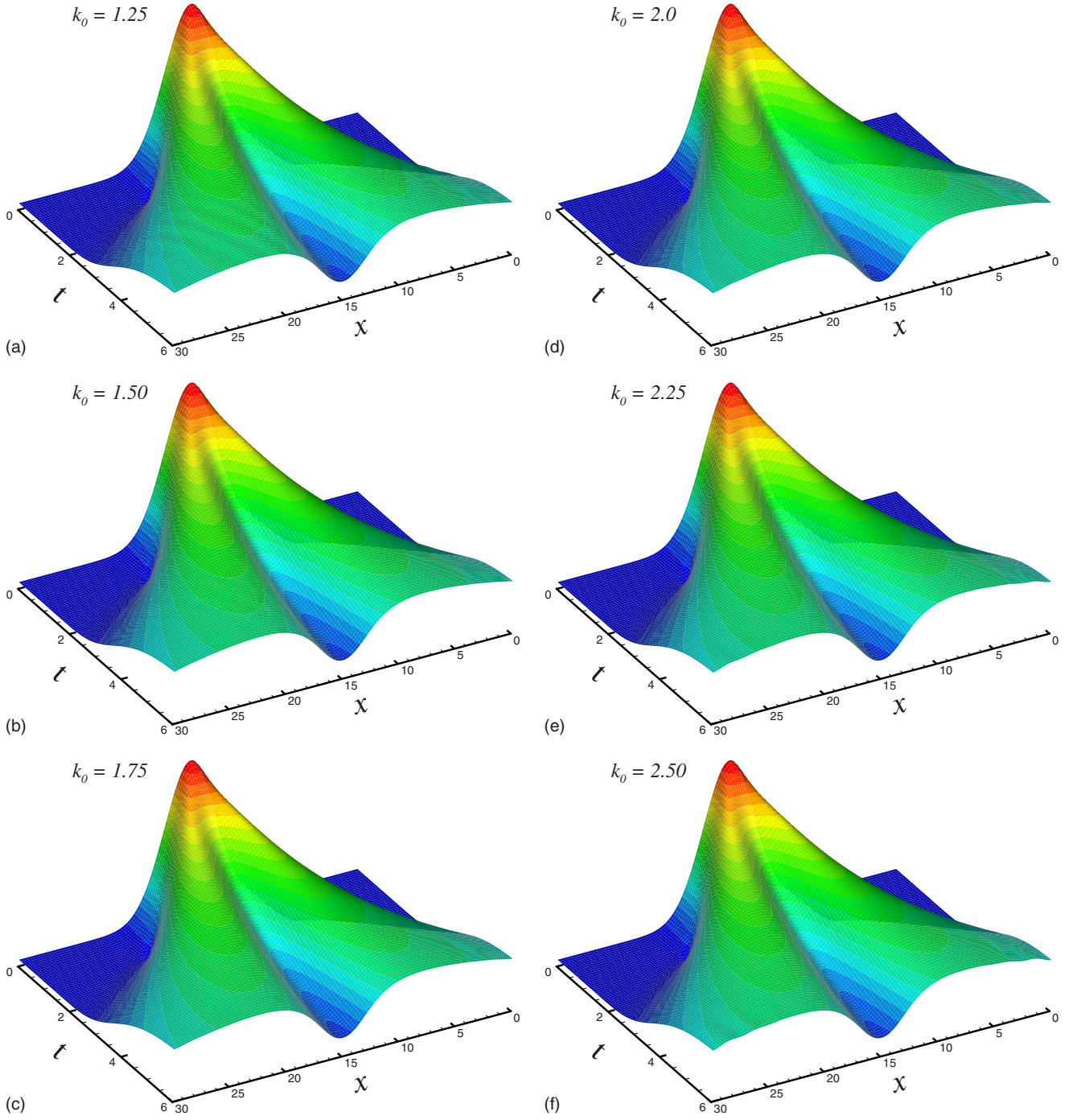

FIG. 6. (Color online) Evolution of the amplitude of the matter wave with ABCs for different k_0.

$$\psi(x,0) = e^{-0.1(x-x_0)^2} \text{ and } V(x) = e^{-0.5(x-x_0)^2}, \quad (41)$$

with $x_0=15$. There is an example in [33,34] to model the expansion of a Bose-Einstein condensate composed of waves with different group velocities. In the calculation, we choose $L=30$, $\Delta x=0.1$, and $\Delta t=0.0375$. Figures 6(a)–6(f) depict the evolution of the wave amplitude with the third-order nonlinear ABCs for different wave numbers k_0. We emphasize the very small spurious reflections by highlighting the figures, which can make us visualize them by showing the associated shadow zones. And the reflective waves are too small to be seen with wave numbers chosen in the appropriate range [1.25, 2]. In Figs. 6(c) and 6(d), no observable reflection can be detected at all. If we take the boundary conditions as a Dirichlet or Neumann boundary condition, the reflective wave is very large (see Ref. [33]) at $t=6$ with the same meshes.

We remark that picking a suitable wave number k_0 in the nonlinear ABCs plays a very important role if we want to obtain an efficient nonlinear absorbing boundary condition. The ideal wave number k_0 is equal to half of the group velocity when a single solitary wave impinges on the boundary.

For an arbitrary wave packet, a suitable wave number can be picked adaptively by using the Gabor transform [34] to capture local frequency information in the vicinity of the artificial boundary, which we will not discuss in this paper.

IV. CONCLUSION

Through approximating the kinetic energy term by a one-way equation and uniting it with the potential energy equation, we proposed an efficient method for designing absorbing boundary conditions of nonlinear Schrödinger equations. The obtained boundary conditions, which are of nonlinear form, can perfectly absorb the outgoing waves. We examined that the coupling between the equation governing the wave in the computational domain and the boundary conditions on the boundary yielded a well-posed problem in a sufficiently small time interval. Furthermore, some numerical examples are given to demonstrate the effectiveness and tractability of the artificial boundary conditions.

ACKNOWLEDGMENTS

The authors would like to thank Professor Houde Han for fruitful discussion on designing the nonlinear ABCs. This research was supported in part by RGC of Hong Kong and FRG of Hong Kong Baptist University.

[1] G. P. Agrawal, *Nonlinear Fiber Optics*, 3rd Ed. (Academic Press, San Diego, 2001).
[2] L. P. Pitaevskii and S. Stringari, *Bose-Einstein Condensation* (Oxford University Press, Oxford, 2003).
[3] C. Sulem and P. L. Sulem, *The Nonlinear Schrödinger Equation: Self-Focusing and Wave Collapse* (Springer, New York, 1999).
[4] M. M. Cerimele, M. L. Chiofalo, F. Pistella, S. Succi, and M. P. Tosi, Phys. Rev. E **62**, 1382 (2000).
[5] S. K. Adhikari, Phys. Rev. E **62**, 2937 (2000).
[6] W. Bao, D. Jaksch, and P. A. Markowich, J. Comput. Phys. **187**, 318 (2003).
[7] Y. B. Gaididei, J. Schjodt-Eriksen, and P. L. Christiansen, Phys. Rev. E **60**, 4877 (1999).
[8] B. Enguist and A. Majda, Math. Comput. **31**, 629 (1977).
[9] R. L. Higdon, Math. Comput. **47**, 437 (1986).
[10] H. D. Han and X. N. Wu, J. Comput. Math. **3**, 179 (1985).
[11] D. H. Yu, J. Comput. Math. **3**, 219 (1985).
[12] L. Halpern and J. Rauch, Numer. Math. **71**, 185 (1995).
[13] H. Han and Z. Huang, Comput. Math. Appl. **44**, 655 (2002).
[14] D. Givoli, *Numerical Methods for Problems in Infinite Domains* (Elsevier, Amsterdam, 1992).
[15] S. V. Tsynkov, Appl. Numer. Math. **27**, 465 (1998).
[16] T. Hagstrom, Acta Numerica **8**, 47 (1999).
[17] H. Han, *Frontiers and Prospects of Contemporary Applied Mathematics* (Higher Education Press and World Scientific, Singapore, 2006), p. 33.
[18] X. Antoine, A. Arnold, C. Besse, M. Ehrhardt, and A. Schädle, Comm. Comp. Phys. **4**, 729 (2008).
[19] S. Jiang and L. Greengard, Comput. Math. Appl. **47**, 955 (2004).
[20] S. Jiang and L. Greengard, Commun. Pure Appl. Math. **61**, 261 (2008).
[21] J. P. Bérenger, J. Comput. Phys. **114**, 185 (1994).
[22] T. Hagstrom and H. B. Keller, Math. Comput. **48**, 449 (1987).
[23] H. D. Han, X. N. Wu, and Z. L. Xu, J. Comput. Math. **24**, 295 (2006).
[24] X. N. Wu and J. W. Zhang, Comput. Math. Appl. **56**, 242 (2008).
[25] Z. Xu, H. Han, and X. Wu, Comm. Comp. Phys. **1**, 479 (2006).
[26] C. Zheng, J. Comput. Phys. **215**, 552 (2006).
[27] X. Antoine, C. Besse, and S. Descombes, SIAM (Soc. Ind. Appl. Math.) J. Numer. Anal. **43**, 2272 (2006).
[28] J. Szeftel, Comput. Methods Appl. Mech. Eng. **195**, 3760 (2006).
[29] J. Szeftel, Numer. Math. **104**, 103 (2006).
[30] A. Soffer and C. Stucchio, J. Comput. Phys. **225**, 1218 (2007).
[31] C. Farrell and U. Leonhardt, J. Opt. B: Quantum Semiclassical Opt. **7**, 1 (2005).
[32] C. Zheng, J. Comput. Phys. **227**, 537 (2007).
[33] Z. Xu and H. Han, Phys. Rev. E **74**, 037704 (2006).
[34] Z. Xu, H. Han, and X. Wu, J. Comput. Phys. **225**, 1577 (2007).
[35] C. Zheng, Comm. Comp. Phys. **3**, 641 (2008).
[36] T. Fevens and H. Jiang, SIAM J. Sci. Comput. (USA) **21**, 255 (1999).
[37] H. O. Kreiss and J. Lorenz, *Initial Boundary–Value Problems and the Navier–Stokes Equations*, (Academy Press, Boston, 1989).
[38] Q. Chang, E. Jia, and W. Sun, J. Comput. Phys. **148**, 397 (1999).
[39] M. Delfour, M. Fortin, and G. Payre, J. Comput. Phys. **44**, 277 (1981).
[40] A. Duán and J. M. Sanz-Serna, IMA J. Numer. Anal. **20**, 235 (2000).
[41] Rémi Carles, SIAM J. Math. Anal. **35**, 823 (2003).
[42] J.-P. Kuska, Phys. Rev. B **46**, 5000 (1992).